BIOCHEMISTRY
including biophysical chemistry & molecular biology

Article

pubs.acs.org/biochemistry

Niemann–Pick Type C Disease: A QM/MM Study of Conformational Changes in Cholesterol in the NPC1(NTD) and NPC2 Binding Pockets

Nadia Elghobashi-Meinhardt*

Department of Chemistry and Biochemistry, Freie Universität Berlin, 14195 Berlin, Germany

Supporting Information

ABSTRACT: Niemann–Pick Type C disease is characterized by disrupted lipid trafficking within the late endosomal (LE)/lysosomal (Lys) cellular compartments. Cholesterol transport within the LE/Lys is believed to take place via a concerted hand-off mechanism in which a small (131aa) soluble cholesterol binding protein, NPC2, transfers cholesterol to the N-terminal domain (NTD) of a larger (1278aa) membrane-bound protein, NPC1(NTD). The transfer is thought to occur through the formation of a stable intermediate complex NPC1(NTD)–NPC2, in which the sterol apertures of the two proteins align to allow passage of the cholesterol molecule. In the working model of the NPC1(NTD)–NPC2 complex, the sterol apertures are aligned, but the binding pockets are bent with respect to one another. In order for cholesterol to slide from one binding pocket to the other, a conformational change must occur in the proteins, in the ligand, or in both. Here, we investigate the possibility that the ligand undergoes a conformational change, or isomerization, to accommodate the bent transfer pathway. To understand what structural factors influence the isomerization rate, we calculate the energy barrier to cholesterol isomerization in both the NPC1(NTD) and NPC2 binding pockets. Here, we use a combined quantum mechanical/molecular mechanical (QM/MM) energy function to calculate the isomerization barrier within the native NPC1(NTD) and NPC2 binding pockets before protein–protein docking as well as in the binding pockets of the NPC1(NTD)–NPC2 complex after docking has occurred. The results indicate that cholesterol isomerization in the NPC2 binding pocket is energetically favorable, both before and after formation of the NPC1(NTD)–NPC2 complex. The NPC1(NTD) binding pocket is energetically unfavorable to conformational rearrangement of the hydrophobic ligand because it contains more water molecules near the ligand tail and amino acids with polar side chains. For three NPC1(NTD) mutants investigated, L175Q/L176Q, L175A/L176A, and E191A/Y192A, the isomerization barriers were all found to be higher than the barrier calculated in the NPC2 binding pocket. Our results indicate that cholesterol isomerization in the NPC2 binding pocket, either before or after docking, may ensure an efficient transfer of cholesterol to NPC1(NTD).

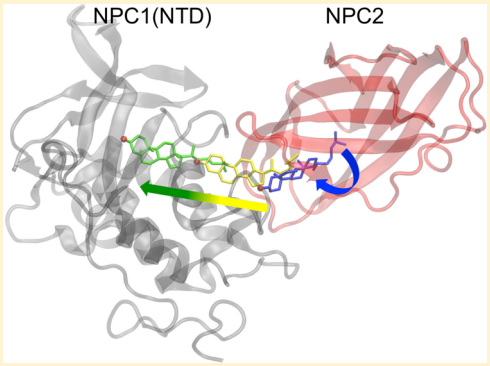

The proper uptake and processing of cholesterol in mammalian cells is required for the viability of the organism. The cellular metabolism of lipids in the late endosomal (LE)/lysosomal (Lys) compartments results in production of cholesterol.[1] After leaving the LE/Lys, cholesterol functions in several capacities: in cell membranes to ensure proper permeability and structural integrity, as a signaling molecule for other cell processes, and as a precursor for the production of steroid hormones.[2] Two proteins, Niemann–Pick type C1 (NPC1) and Niemann–Pick type C2 (NPC2), have been identified for being responsible for transporting cholesterol in and out of the LE/Lys compartments. Mutations in either NPC1 or NPC2 lead to an accumulation of cholesterol and lipids in the LE/Lys, the primary characteristic of Niemann–Pick type C (NPC) disease.[3]

For individuals carrying NPC disease, 95% of cases are due to a mutation in NPC1, and only 5% of cases arise from mutations in the NPC2. The resulting cholesterol accumulation in organs of patients with the NPC disease often has severe consequences. In cases in which the disease manifests itself at birth, the outcome after neurological deterioration is almost always death during early childhood. Clinical procedures have been established to ascertain the presence of NPC in patients, a databank of genetic mutations has been tabulated,[4] some therapeutic strategies have been proposed and tested.[5] However, despite extensive genetic testing, little is known about the behavior of the NPC1 and NPC2 proteins on a molecular level. Furthermore, mechanistic hypotheses regarding the uptake and transfer of cholesterol have only recently begun to be investigated using computational modeling.[8]

Cholesterol transport within the lysosome is thought to occur as follows. Low-density lipoprotein (LDL) contains 500 molecules of free cholesterol and 1500 molecules of esterified cholesterol that are hydrolyzed by acid lipase in the lysosome lumen.[6] NPC2, a small (131aa) soluble protein that is completely free in the lumen, first accepts cholesterol.

Received: May 8, 2014
Revised: September 24, 2014
Published: September 24, 2014

   dx.doi.org/10.1021/bi500548f | *Biochemistry* 2014, 53, 6603–6614

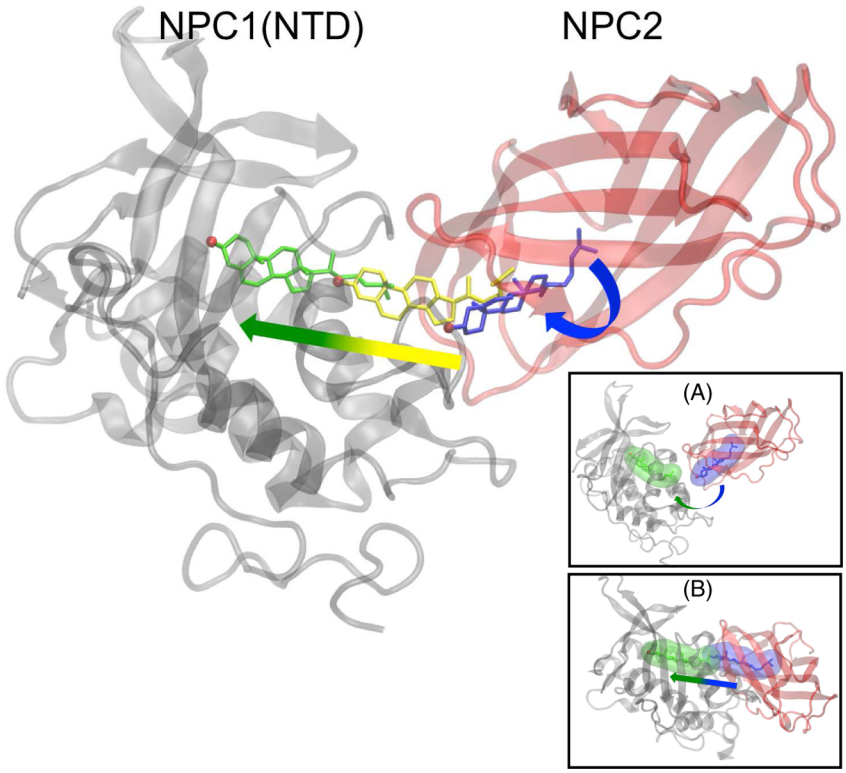

Figure 1. The NPC1(gray)−NPC2(red) protein complex, based on a working model of Brown, Goldstein, and co-workers,[12] is depicted in a ribbon representation. (Initial coordinates were adapted from ref 8.) In the NPC2 binding pocket, the sterol (blue stick representation) tail is buried in the binding pocket, and the 3β-hydroxyl group (red ball) extends toward the NPC1 binding pocket. In NPC1(NTD), the orientation of the ligand (green stick representation) is reversed, with the ligand 3β-hydroxyl group (red ball) pointing toward the interior of the protein, while the isooctyl sterol tail points toward the sterol opening. The transfer of the cholesterol ligand from one binding pocket to the other requires a conformational change in the ligand−protein complex. One possible mechanism includes the conformational rearrangement of cholesterol inside the NPC2 binding pocket (indicated with blue arrow) to form an intermediate structure (yellow), followed by ligand transfer to the NPC1 binding pocket (yellow to green arrow). Inset (A) shows that the NPC2 binding pocket (highlighted in blue) and the NPC1 binding pocket (highlighted in green) in the working model of ref 8 are bent with respect to each other and indicates the presumed path for ligand transfer (blue to green arrow). Inset (B) shows an alternative scenario in which the protein moieties are rotated with respect to one another such that the binding pockets are arranged in a linear fashion. The transfer of the cholesterol ligand in such a model would require minimum conformational change in the ligand.

Hydrophobic amino acids forming an apolar rim of the binding entrance (V59, V64, F66, Y100, P101, I103) are believed to allow for lengthwise insertion of the hydrophobic sterol tail into the opening rather than the hydroxyl group entering the cavity first.[7]

The transfer of cholesterol to NPC1(NTD) is thought to occur when NPC2 binds to a second luminal loop-domain of the membrane-bound NPC1 protein (NPC1(D2) [residues 372−622]).[13] The docking of the two NPC proteins allows the hydrophobic sterol molecule to slide from NPC2 to NPC1-(NTD) without exposure to the aqueous phase in the lysosome's interior.[14,15] This sliding model is supported by crystallographic data that show the opposite orientation of cholesterol in the respective binding sites of NPC1(NTD)[10] and NPC2.[14] It is hypothesized that, after leaving the N-terminal domain of NPC1, cholesterol passes through the bilayer of the lysosomal limiting membrane. This may occur via a sterol-sensing domain in the NPC1 protein (NPC1(SSD) [residues 372−622]) that consists of five membrane-spanning domains that has high homology to that of other cholesterol-regulating proteins such as HMG-CoA-reductase (HMGCR) or SCAP.[11] Alternatively, participation of one to several other yet unidentified proteins may play a role. Additional lipid binding proteins could also facilitate the transport of cholesterol from lysosomal limiting membranes to acceptor membranes in other organelles.

Molecular structures of the NPC1 (1278aa) and NPC2 (131aa) proteins have recently been generated. X-ray crystallography has revealed high-resolution structural data of the relatively small NPC2 protein in the apo form [PDB: 1NEP][9] and with cholesterol bound [PDB: 2HKA].[7] Of the much larger NPC1 protein, only the structure of N-terminal domain NPC1(NTD) (240aa [residues 25−264]) has been elucidated to date.[10] NPC1(NTD) binds both cholesterol and oxygenated derivatives of cholesterol, in particular 25 hydroxycholesterol (25-HC) and 27-hydroxycholesterol (27-HC), with high affinity, and PDB structures exist for the apo structure [PDB: 3GKH], the cholesterol-bound structure [PDB: 3GKI], and the 25-HC-bound structure [PDB: 2GKJ].[10]

An X-ray crystal structure of the NPC1(NTD)−NPC2 complex has not yet been generated, but using X-ray crystallography data of the two individual proteins, Brown, Goldstein, and co-workers have constructed a working model of the NPC1(NTD)−NPC2 protein complex.[12] In the model, the sterol apertures are aligned, but the binding pockets are approximately 100° bent with respect to one another[12] (Figure 1). Therefore, after protein−protein docking, transfer of cholesterol from NPC2 to NPC1(NTD) requires either that the protein backbone shift to allow ligand passage and/or that

dx.doi.org/10.1021/bi500548f | Biochemistry 2014, 53, 6603−6614

the ligand undergo a conformational change in order to slide from one binding pocket to the other. In the latter case, since the cholesterol's ring system is rigid, the flexible isooctyl tail must twist to accommodate the bent transfer pathway (Figure 2).

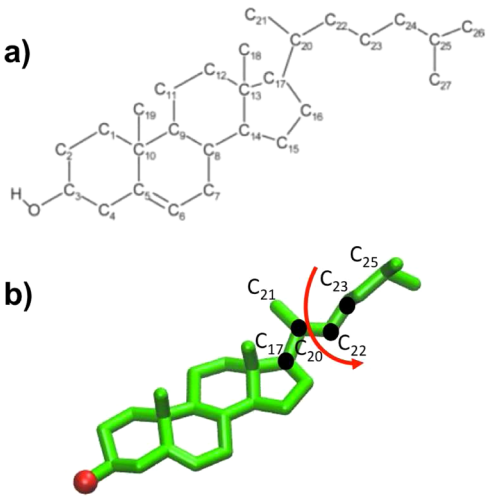

Figure 2. (a) Stick model of cholesterol molecule with carbon positions labeled. (b) Model of cholesterol with carbon atoms shown in green and oxygen atom shown in red. Isomerization of the C_{17}–C_{20}–C_{22}–C_{23} segment in the counterclockwise direction is indicated with a red arrow.

Indeed, it is known that the sterol opening of NPC1(NTD) is too small to allow passage of the sterol ligand without a conformational change in either the protein, the ligand, or both.[10] In fact, the NPC1(NTD) binding pocket exists in a relatively closed conformation but can be opened by the presence of NPC2.[12] Kinetic studies show that the presence of NPC2 markedly accelerates the binding and release of cholesterol from NPC1(NTD).[12] At 37 °C, NPC1(NTD) binds cholesterol on the order of 10–15 s.[12] In the absence of NPC2, the rate slows by a factor of 140,[12] strongly suggesting that NPC2 facilitates the transfer of cholesterol in living cells by complexing with NPC1(NTD) and initiating a conformational change in the ligand–protein–protein complex.

In a recent theoretical study, Wiest and co-workers performed extensive classical molecular dynamics (MD) simulations on the binding process and the cholesterol transfer.[8] For their simulations, they used the apo- and ligand-bound forms of the NPC1(NTD)–NPC2 complex based on the working model of Brown, Goldstein, and co-workers.[8] The two ligand-bound NPC1(NTD)–NPC2 complexes show some differences. Inside the NPC1(NTD) binding pocket, the sterol molecule 3β-hydroxyl group points toward the interior of the binding pocket, whereas inside the NPC2 binding pocket, the sterol molecule has the opposite orientation, with the hydroxyl group pointing toward the sterol opening. Also, the conformation of the isooctyl tail differs in the two binding pockets. In the crystal structures of the uncomplexed NPC1(NTD) and NPC2 proteins, 3GKI[10] and 2HKA,[7] respectively, the dihedral angle of the C_{17}–C_{20}–C_{22}–C_{23} segment is nearly identical (−164°), suggesting that the cholesterol ligand adopts a similar geometry in both proteins in the uncomplexed state. However, in the protein–protein complex of ref 8, the dihedral angle of the C_{17}–C_{20}–C_{22}–C_{23} segment in NPC1 is −157.3°, and in NPC2, it is 71.6°. This changed ligand conformation raises the question of whether, following protein–protein complexation, the cholesterol ligand undergoes a conformational change that is subsequently required for transfer. After cholesterol transfer, the NPC1(NTD)–NPC2 complex dissociates, with cholesterol remaining in the binding pocket of NPC1(NTD).[8] The geometry of cholesterol after protein–protein dissociation is unknown, but it is likely that the ligand relaxes to a conformation close to the native geometry found in the crystal structure.

The steps required for the successful docking of NPC1(NTD) and NPC2 proteins and subsequent ligand transfer are largely unknown. One possibility is that the soluble NPC2 protein, following uptake of cholesterol, initiates a conformational rearrangement of the ligand and/or the protein which is required for the subsequent transfer to the NPC1(NTD) binding pocket (Figure 3A). Alternatively, docking of NPC2 to

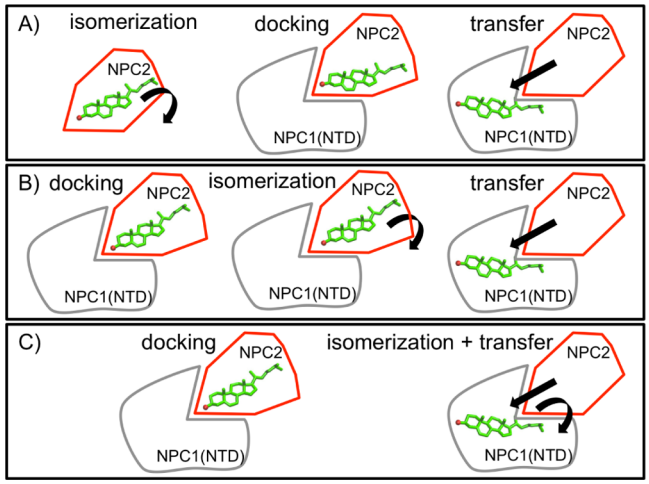

Figure 3. Possible cholesterol transfer mechanisms include (A) cholesterol isomerization in free NPC2 followed by protein–protein docking and cholesterol transfer, (B) protein–protein docking followed by cholesterol isomerization and transfer, and (C) protein–protein docking followed by combined cholesterol transfer and isomerization.

NPC1(NTD) could trigger a conformational change in the ligand and/or the proteins, thereby preparing the system for ligand transfer (Figure 3B). A third possibility is that the cholesterol ligand and proteins simultaneously undergo conformational changes while the ligand is transferred from one binding pocket to the next (Figure 3C). To check the range of conformational freedom within the two binding pockets, 20 ns classical MD simulations were carried out with the cholesterol ligand in each of the binding pockets of the NPC1(NTD)–NPC2 complex (details of MD simulation are given in the Methods). The sterol tail was observed to sample a range of dihedral angles (Figure 4). These conformational changes in the ligand geometry, similarly observed in the work of Wiest and co-workers,[8] raise the question of whether cholesterol isomerization plays a role in the transfer mechanism.

To address this question, here we examine in detail the conformational rearrangement of the sterol ligand inside the protein binding pockets both before and after protein–protein complexation has occurred. In other words, cholesterol isomerization is studied in the free NPC1(NTD) and NPC2

dx.doi.org/10.1021/bi500548f | Biochemistry 2014, 53, 6603–6614

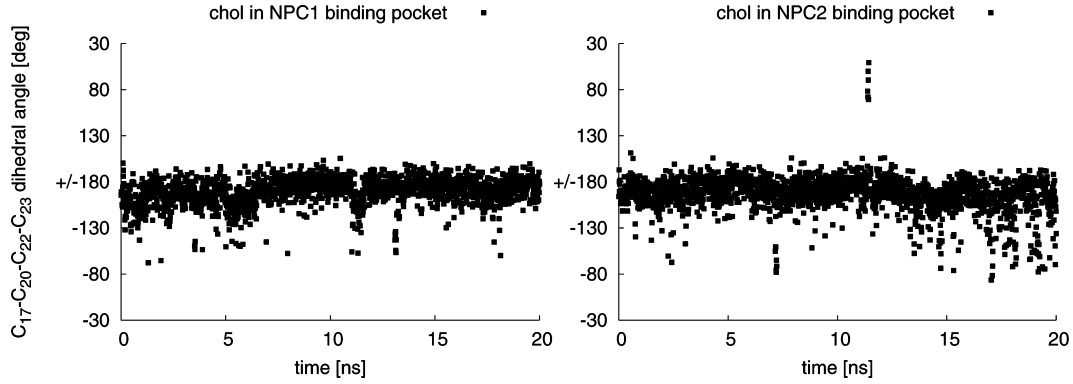

Figure 4. Range of dihedral angles (C_{17}−C_{20}−C_{22}−C_{23} cholesterol fragment) sampled over 20 ns classical MD simulations of NPC1/chol−NPC2 (left) and NPC1−NPC2/chol (right) complexes carried out at 310 K.

binding pockets as well as in both binding pockets of the NPC1(NTD)−NPC2 protein complex. Our aim is to calculate the energy barrier associated with the isomerization of the sterol ligand and to investigate structural features of the two binding pockets that affect the energy barrier. For each of the two binding pockets, we calculate the isomerization energy barrier while tracking conformational changes in the surrounding protein and water molecules that accompany the reaction. A characterization of these processes on the molecular level will provide insight into the complex problem of cholesterol transfer between NPC2 and NPC1(NTD).

We use a hybrid quantum mechanical/molecular mechanical (QM/MM) energy function[16−18] to calculate the energy barrier associated with cholesterol isomerization in both binding pockets. In our calculations, the cholesterol ligand is treated with QM, and the surrounding protein and water molecules are treated with MM. The QM method is chosen over a classical force field in order to describe more accurately the torsional strain of the isomerizing isooctyl tail of the ligand. A QM/MM energy term accounts for the electrostatic and van der Waals interactions between the sterol ligand and the surrounding protein and water molecules. For NPC1(NTD), we investigate the wild-type protein as well as three mutants, L175Q/L176Q, L175A/L176A, and E191A/Y192A, whose side chains are located in the sterol binding pocket. Highly conserved in multiple mammalian species,[10] these mutants have been identified as being the most deficient in restoring egress of cholesterol from lysosomes.[10,14] We analyze the effect of amino acid mutations on binding pocket geometry and isomerization energy barriers.

For clarity of notation, NPC1(NTD) will henceforth be referred to as NPC1. For the case in which cholesterol is in the NPC1 binding pocket, the notation will be NPC1/chol. Similarly, cholesterol located in the NPC2 binding pocket is notated as NPC2/chol. The protein−protein complexes are notated as NPC1/chol−NPC2 and NPC1−NPC2/chol.

METHODS

Construction of Models. We investigate the NPC1 and NPC2 proteins before docking (free) and after docking (protein−protein complex). For the free NPC1 and NPC2 proteins, models were constructed from the existing crystal structures. A model of the wild-type NPC1 protein bound to cholesterol was constructed based on the 3GKI crystal structure, which includes 100 water molecules.[10] The NPC1 contains amino acid residues 23−247.[10] For NPC2, the structure was based on PDB structure 2HKA containing amino acid residues 1−130 and 110 water molecules; the cholesterol sulfate was converted to cholesterol.[7] For the protein−protein complexes, we modeled the NPC1−NPC2 complex with cholesterol in the NPC1 and NPC2 binding pockets, respectively, by positioning the two individual protein crystal structures with their respective water molecules using the complex of ref 8 as a template. Any water molecule from one PDB structure that was overlapping with a water molecule from the other PDB structure was deleted (approximately 10−20 molecules occurring near the interface of the two crystal structures). Water molecules in the protein binding pockets, as found in the crystal structures, were not affected by the protein−protein complexation and remained unchanged. The geometry of the cholesterol ligand inside the binding pockets for NPC1 and NPC2 was the original geometry from the crystal structures 3GKI[10] and 2HKA,[7] respectively.

Three NPC1 mutant protein−protein complexes were investigated: L175Q/L176Q, L175A/L176A, and E191A/Y192A. To construct the models, the side chains of the native 3GKI crystal structure were mutated *in silico* using CHARMM. The NPC1/chol−NPC2 complex was then constructed in an identical fashion as that for the native protein−protein complex, namely, by positioning the mutant NPC1 and native NPC2 crystal structures using the complex of ref 8 as a template. As in the case of the native protein−protein complex, any water molecule from the one crystal structures that was overlapping with a water molecule from the crystal structure was deleted, but water molecules in the binding pockets were not affected. The cholesterol ligand was located in the NPC1(NTD) binding pocket of each of the three mutants. Thus, a total of five protein−protein complexes were constructed: four protein−protein complexes containing the ligand in the NPC1 binding pocket (native NPC1/chol−NPC2, L175Q/L176Q, L175A/L176A, E191A/Y192A) and one complex, native NPC1−NPC2/chol, containing the cholesterol ligand in the NPC2 binding pocket.

Hydrogen atoms were added using H-build from CHARMM.[19] The N-terminus was capped with a neutral group CH_3−CO−, and the C-terminus was capped with the neutral methyl acetate −NH−CO−OCH_3. According to the crystal structures, nine disulfide bonds involving 18 cysteine residues of NPC1(NTD) (Cys25−Cys74, Cys31−Cys42, Cys63−Cys109, Cys75−Cys113, Cys97−Cys238, Cys100−Cys160, Cys177−Cys184, Cys227−Cys243, Cys240−Cys247) and three disulfide bonds involving six cysteine residues of

dx.doi.org/10.1021/bi500548f | *Biochemistry* 2014, 53, 6603−6614

NPC2 (Cys8−Cys121,Cys23−Cys28,Cys74−Cys80) were constructed using CHARMM. For the initital modeling of cholesterol, the corresponding topology and force field parameters were developed and optimized at the DFT(B3LYP) level and included in CHARMM.[20,21] Unless otherwise noted, all subsequent energy calculations treated the cholesterol ligand using quantum mechanics, as discussed in the following section.

Potential Energy Function. All computations reported here were performed using a quantum mechanical/molecular mechanical (QM/MM) Hamiltonian.[16−18] In the QM/MM approach, the active site of a protein is treated with QM, and the remainder of the protein is described with MM. The total energy is given by

$$E = E_{QM} + E_{MM} + E_{QM/MM} \quad (1)$$

where E_{QM} includes the electronic energy of the QM atoms for a given nuclear configuration, E_{MM} describes the classical interactions between the MM atoms, and $E_{QM/MM}$ represents the interaction between the QM and MM atoms. The $E_{QM/MM}$ term can be further decomposed into the following three terms

$$\begin{aligned} E_{QM/MM} &= E^{bond}_{QM/MM} + E^{Coul}_{QM/MM} + E^{vdW}_{QM/MM} \\ &= E^{bond}_{QM/MM} + E^{nb}_{QM/MM} \end{aligned} \quad (2)$$

where $E^{bond}_{QM/MM}$ is the energy due to bonded atoms at the QM/MM interface, and the nonbonded QM/MM energies, $E^{Coul}_{QM/MM}$ and $E^{vdW}_{QM/MM}$, are, respectively, the Coulombic and van der Waals interactions between QM and MM atoms. MM atoms were treated using the CHARMM27 parameter set for the protein[22] and the TIP3P model for water molecules.[23]

The QM region was treated using the self-consistent-charge density functional tigh binding (SCC-DFTB) method,[24] as implemented in the CHARMM package.[19] SCC-DFTB has been shown to reproduce the B3LYP/6-31G(d,p) geometries of small hydrocarbons[25,26] and to give the correct ordering of relative energies of conformations of small peptides.[27] In molecules containing a polyene system of conjugated bonds, SCC-DFTB has proven to be accurate in describing the torsional barriers of single and double bonds.[28] All QM/MM computations reported here were performed with a QM region consisting of the cholesterol ligand. The remainder of the simulation system was treated using MM.

Geometry Optimization of Initial Structures. After construction of the native and mutant protein structures from the respective crystal structures, the free proteins and the protein−protein complexes were geometry-optimized as follows. In the first step, the hydrogen atom positions were optimized using an MM potential, keeping the heavy atoms and water oxygen atoms fixed. In the second step, we optimized the protein geometry using a harmonic force constraint of 1.0 kcal/mol·Å^2 on the α-carbon and water oxygen atoms. Next, using a hybrid QM/MM potential, the coordinates of the QM atoms were then optimized by keeping the MM atoms fixed. In the fourth step, we defined a mobile region that included the cholesterol ligand and all protein amino acids within a 15 Å radius of the cholesterol ligand. In the cases with cholesterol in the NPC1(NTD) binding pocket, the mobile region (a total of 3449 atoms) included residues 162−186, which are believed to undergo conformational change, thereby opening the NPC1 pocket and enabling cholesterol transfer. In the case with cholesterol in the NPC2 binding pocket, the mobile region consisted of 3779 atoms. With all other atoms held fixed, the positions of all mobile residue atoms were optimized without constraints to a gradient limit value of 10^{-3} kcal/mol/Å.

Isomerization Reaction. Isomerization calculations were performed for each of the two free proteins, NPC1 and NPC2, as well as for five protein−protein complexes (Table 1): The

Table 1. Seven Isomerization Reactions Studied Here[a]

structure	description
	Cholesterol in NPC1 Binding Pocket
1	NPC1/chol (free)
2	NPC1/chol−NPC2 (complex)
3	L175Q/L176Q NPC1/chol−NPC2 (complex)
4	L175A/L176A NPC1/chol−NPC2 (complex)
5	E191A/Y192A NPC1/chol−NPC2 (complex)
	Cholesterol in NPC2 Binding Pocket
6	NPC2/chol (free)
7	NPC1−NPC2/chol (complex)

[a]Five isomerization reactions contained the cholesterol ligand in the NPC1 binding pocket and two contained the cholesterol ligand in the NPC2 binding pocket.

starting structure for each set of calculations was the relaxed ligand−protein structure, as obtained from the energy minimization calculations during structure preparation (see Geometry Optimization of Initial Structures). For all structures, the initial dihedral angle of the $C_{17}-C_{20}-C_{22}-C_{23}$ fragment was varied in 5° increments from −180° to +180°. At each dihedral angle value, a harmonic restoring force of 50 kcal/mol·deg^2 was applied to constrain the dihedral angle of the $C_{17}-C_{20}-C_{22}-C_{23}$ segment to the sampling value. All mobile residue atoms, as defined in the initial energy minimization (Geometry Optimization of Initial Structures), were kept unconstrained while the remainder of the protein was held fixed. A QM/MM energy minimization using the adopted basis Newton−Raphson (ABNR)[19] minimization was carried out for each dihedral angle value along the isomerization trajectory. Each starting structure was energy-minimized to a gradient limit value of 0.01 kcal/mol/Å. To check convergence of energy values, extensive preliminary tests were carried out to test the harmonic restoring force and RMS gradient limit value. Changing the harmonic force constant of 50 kcal/mol·deg^2 by a factor of 10 led to a change of less than 1 kcal/mol in isomerization barrier height. Changing the gradient tolerance from 0.01 kcal/mol/Å by a factor of 10 led to 1−2 kcal/mol changes in barrier heights, on the order of 10% of the SCC-DFTB rotational energy barrier.[28]

Molecular Dynamics Simulations. MD simulations (20 ns) were carried out for both NPC1/chol−NPC2 and NPC1−NPC2/chol complexes with NAMD[29] using the CHARMM all-atom force field.[22] Each protein−protein complex was placed in a rectangular box (100 × 75 × 55 Å^3) containing explicit solvent molecules (12 786 TIP3 water molecules[23]). To simulate a continuous system, periodic boundary conditions were applied. The MD simulations used an integration time step of 2 fs and the SHAKE algorithm[30] to constrain all bonds involving hydrogen atoms. A nonbonded cutoff of 10.0 Å was used, and the nonbonded pair list was updated every 10 time steps. The temperature (310 K) was controlled using Langevin dynamics, with a collision frequency of 1.0 ps^{-1} and isotropic position scaling to maintain pressure (1 atm).[31]

Reaction Pathway Calculations. To check the validity of the reaction coordinate ($C_{17}-C_{20}-C_{22}-C_{23}$ dihedral angle), a

dx.doi.org/10.1021/bi500548f | Biochemistry 2014, 53, 6603−6614

Table 2. Comparison of Cholesterol $C_{17}-C_{20}-C_{22}-C_{23}$ Dihedral Angle Values[a]

structure	$C_{17}-C_{20}-C_{22}-C_{23}$ dihedral angle (deg)	protein backbone RMSD from complex of ref 8 (Å)
Cholesterol in NPC1		
NPC1/chol [PDB: 3GKI][10]	−163.9	
NPC1/chol (QM/MM)	−165.6	0.54 (reference PDB: 3GKI[10])
NPC1/chol–NPC2 (QM/MM)	−173.8	1.70
NPC1/chol–NPC2 (classical)	−170.5	1.78
NPC1/chol–NPC2[8]	−157.3	0.00
L175Q/L176Q mutant NPC1/chol–NPC2	−174.9	1.27
L175A/L176A mutant NPC1/chol–NPC2	−174.9	1.27
E191A/Y192A mutant NPC1/chol–NPC2	−162.1	1.28
Cholesterol in NPC2		
NPC2/chol [PDB: 2HKA][7]	−164.4	
NPC2/chol (QM/MM)	−157.0	0.41 (reference PDB: 2HKA[7])
NPC1–NPC2/chol (QM/MM)	−156.5	1.83
NPC1–NPC2/chol (classical)	−174.0	1.89
NPC1–NPC2/chol[8]	71.6	0.00

[a]Unless otherwise noted, all values reported from this study are obtained from the final relaxed protein–ligand structure calculated using the QM/MM energy function and minimization procedure discussed in the Methods. For comparison, geometry optimizations of the two protein–protein complexes were perfomred using a purely classical energy function with all atoms treated with the CHARMM27 parameter set.[22] The dihedral angle values reported from ref 8 correspond to final geometries after classical MD simulations using the AMBER11 force field.[33]

reaction pathway calculation for the isomerization reaction in the NPC1/chol–NPC2 complex was computed with the conjugate peak refinement (CPR) algorithm,[32] as implemented in the TREK module of CHARMM.[19] The CPR algorithm computes the first-order saddle points along an adiabatic reaction path that connects the energy-optimized reactant and product states of the reaction (here, cholesterol isomerization).[32] In this method, the system's complex degrees of freedom that can be involved in the reaction path are allowed to vary simultaneously; no *a priori* knowledge of a reaction coordinate is required. The only input required is the energy-optimized reactant and product state structures; these end states are obtained via direct energy optimization (energy gradient limit value of 10^{-3} kcal/mol/Å) of the reactant and product structures, i.e., reactant with $C_{17}-C_{20}-C_{22}-C_{23}$ dihedral angle of −180° and product dihedral angle of 180°, as obtained from the isomerization calculation described above. The computed CPR minimum energy pathway thus yields the intrinsic reaction coordinate connecting reactant and product states as well as the barrier height of the transition state. The CPR method can therefore be considered a method for validating both the choice of reaction coordinate as well the transition state energy barrier calculated for a given reaction coordinate.

RESULTS AND DISCUSSION

Structures. *Free NPC1/chol and Free NPC2/chol.* Table 2 reports cholesterol $C_{17}-C_{20}-C_{22}-C_{23}$ dihedral angle values as obtained from the final relaxed protein–ligand structure calculated using the QM/MM energy function (see Potential Energy Function) and minimization procedure (see Geometry Optimization of Initial Structures) previously discussed. The QM/MM geometry optimized structures of free NPC1/chol and NPC2/chol show minimum deviation from the respective crystal structures,[7,10] with protein backbone RMSDs of 0.54 and 0.41 Å, respectively (Table 2). The geometry of the cholesterol $C_{17}-C_{20}-C_{22}-C_{23}$ segment is, in both cases, close to that of the crystal structure, although a somewhat larger deviation is observed in the case of NPC2.

Native and Mutant NPC1/chol–NPC2 Protein–Protein Complex. All of the QM/MM energy minimized protein–protein complexes remain close to the structures of ref 8, which correspond to end points of classical MD simulations (after 86 ns),[8] although the geometries of the cholesterol isooctyl tail vary between the structures (geometries and protein backbone RMSD values given in Table 2). In the native NPC1/chol–NPC2, the cholesterol 3β-hydroxyl group is buried in the binding pocket, hydrogen bonding via two water molecules with the polar amino acids Asn41 and Gln79 and the negatively charged partially solvent-exposed Glu30 (Figure 5). The cholesterol isooctyl tail is oriented toward the sterol opening of NPC1 and is bent upward relative to the plane of the sterol ring system. Five water molecules are located near the sterol tail, between cholesterol and amino acids of helix 3 (see the inset in Figure 5). The cholesterol C_{21} methyl group is rotated approximately 90° in the clockwise direction relative to the C_{18} and C_{19} methyl groups (see Figure 2 for cholesterol labeling). The binding pockets of the L175Q/L176Q, L175A/L176A, and E191A/Y192A mutants are structurally similar to that of the wild-type (Supporting Information Figure S1). In wild-type NPC1/chol–NPC2, six water molecules are within 4 Å of the cholesterol ligand, in the L175Q/L176Q and L175A/L176A mutants, only four water molecules are within this radius (Supporting Information Figure S1), and in the E191A/Y192A mutant, only three water molecules are observed within 4 Å of the cholesterol ligand, suggesting that all mutations cause a slight shifting of the overall protein structure, allowing the waters to migrate away from the sterol ligand.

Native NPC1–NPC2/chol Protein–Protein Complex. The cholesterol tail in the NPC1–NPC2/chol complex is oriented toward the interior of the NPC2 binding pocket (opposite orientation from the NPC1/chol–NPC2 complex) while the 3β-hydroxyl group extends out of the binding pocket toward the NPC2 sterol opening (Figure 1). The NPC1–NPC2/chol complex of Wiest et al., obtained after 86 ns of MD simulations using the classical AMBER11 force field,[33] shows a significantly different $C_{17}-C_{20}-C_{22}-C_{23}$ dihedral angle 71.6° as compared to −164.4° in the original crystal structure of the cholesterol-bound NPC2 (PDB: 2HKA) of ref 7 and as compared to our

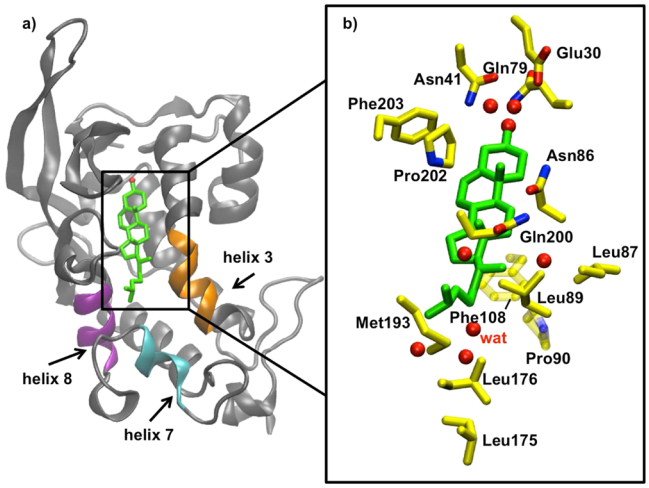

Figure 5. (a) NPC1/chol is represented as a gray ribbon diagram with the cholesterol ligand shown in green and hydroxyl oxygen atom shown in red. Helices 3, 7, and 8, which are the most involved in cholesterol binding and transfer, are highlighted in color. (b) Close-up inset shows cholesterol (green) with functionally important surrounding amino acids (yellow) and oxygen atoms (red) of nearest water molecules after QM/MM energy minimization. The water molecule nearest to the cholesterol tail is marked in red. The cholesterol 3β-hydroxyl group hydrogen bonds with polar residues Asn41 and Gln79 and forms a water-mediated bond with the partially solvent-exposed side chains of Glu30. Hydrophobic amino acids Pro90, Phe108, Leu175, Leu176, and Met193 surround the sterol tail. The polar side chain of Gln200 points away from the ligand. Oxygen atoms are shown in red, and nitrogen atoms are shown in blue.

QM/MM calculated value −156.5° (Table 2). The sterol tail in ref 8 is bent down with respect to the plane of the ring system, unlike that in our complex. In our QM/MM relaxed structure, the sterol ring system is almost planar, with the sterol tail pointing up relative to the plane of the ring system (Figure 6). The cholesterol ligand is surrounded predominantly by amino

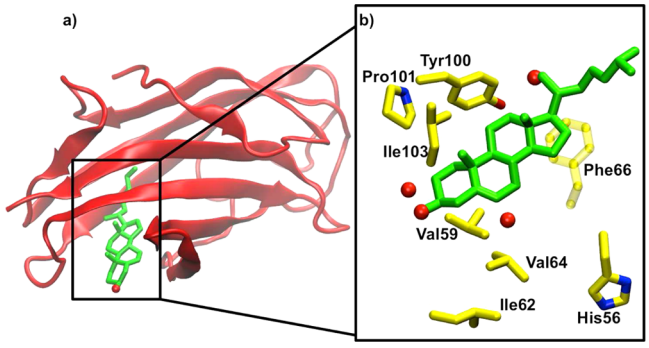

Figure 6. (a) NPC2/chol is represented as a red ribbon diagram with the cholesterol ligand shown in green and 3β-hydroxyl oxygen atom shown in red. (b) Close-up inset shows cholesterol (green) with functionally important surrounding amino acid residues (yellow) and oxygen atoms (red) of nearest water molecules after QM/MM energy minimization. The choleserol hydroxyl group extends out of the NPC2 binding pocket and hydrogen bonds with a nearby water molecule, while the sterol tail is buried inside the binding pocket. The dihedral angle of the C_{17}−C_{20}−C_{22}−C_{23} segment in NPC2 is −157°. Surrounding amino acids that could be involved in ligand transfer include hydrophobic residues Val59, Ile62, Val64, Phe66, Pro101, and Ile103 and one polar amino acid, Tyr100, that hydrogen bonds with a water molecule.

acids with hydrophobic side chains. The hydroxyl group of Tyr100 hydrogen bonds with the nearby water molecule, and the cholesterol 3β-hydroxyl group interacts with a second water molecule near the sterol opening. A third water molecule is located under the plane of the sterol ring system. Compared to the NPC1 binding pocket, the NPC2 binding pocket contains fewer water molecules near the ligand as well as fewer amino acids with polar side chains, both of which are better suited to the hydrophobic nature of the cholesterol molecule.

Isomerization in the NPC1 Binding Pocket. The cholesterol isomerization energy profiles in the NPC1 binding pocket are shown in Figure 7 for the free NPC1/chol protein (red line) and for the NPC1/chol−NPC2 protein complex (green line). The minimum energy of the cholesterol isomerization is located near a C_{17}−C_{20}−C_{22}−C_{23} dihedral angle of −175°. In the free protein, the isomerization of the sterol tail toward 180° proceeds via an energy barrier of 19.5 kcal/mol, whereas in the protein−protein complex, the barrier is 21.8 kcal/mol. The primary contribution to the isomerization barrier in both cases is the QM energy arising from the twisted geometry of the cholesterol ligand that is constrained inside the binding pocket. The lower isomerization energy barrier in the free protein can be explained by considering the flexibility of the protein helices near the sterol aperture. In the free protein, the sterol tail extends toward the aperture that is solvent-exposed, whereas in the NPC1/chol−NPC2 complex, the ligand tail is restricted by the NPC2 protein at the interface, thus reducing the conformational freedom.

Isomerization of the C_{17}−C_{20}−C_{22}−C_{23} fragment is accompanied by a twisting of the adjacent C_{20}−C_{22}−C_{23}−C_{24} and C_{22}−C_{23}−C_{24}−C_{25} segments, causing a rotation of the C_{21} methyl group in the clockwise direction and giving rise to the small sharp peak located near −130° and a small round peak near 110° in the isomerization energy profile (Figure 7). As the ligand tail rotates, the distance changes between the C_{21} methyl group and the helix 3 protein backbone localized on the nearby amino acids Asn86, Leu87, and Leu89 (Figure 5). This observation is consistent with the X-ray crystallography data of the apo- and cholesterol-bound NPC1 structures. which indicate a displacement (1 Å) of helix 3 occurring at Asn86/Leu87.[10]

To check that the C_{17}−C_{20}−C_{22}−C_{23} dihedral angle is a valid reaction coordinate for the isomerization reaction, the isomerization path was recomputed for the NPC1/chol−NPC2 complex using the CPR method (see Methods). Several snapshots of the energy-minimized system from the isomerization profile are used as input structures to compute the minimum-energy path yielding the intrinsic reaction coordinate. The resulting isomerization minimum energy path as a function of the normalized intrinsic coordinate λ shows a barrier (21.9 kcal/mol) nearly identical to the barrier obtained using the C_{17}−C_{20}−C_{22}−C_{23} dihedral angle as a reaction coordinate (Figure 8a). The C_{17}−C_{20}−C_{22}−C_{23}, C_{20}−C_{22}−C_{23}−C_{24}, and C_{22}−C_{23}−C_{24}−C_{25} dihedral angles are observed to undergo simultaneous rearrangement over the course of the reaction (Figure 8b).

To understand the factors influencing the QM/MM energy barrier, for the case of the protein−protein complex we decomposed the total QM/MM energy into the individual energy contributions (Supporting Information Figure S2). The total QM/MM energy proceeds via a barrier of 21.8 kcal/mol before the energy returns to its minimum energy (Supporting Information Figure S2, solid red line). The QM energy is

dx.doi.org/10.1021/bi500548f | Biochemistry 2014, 53, 6603−6614

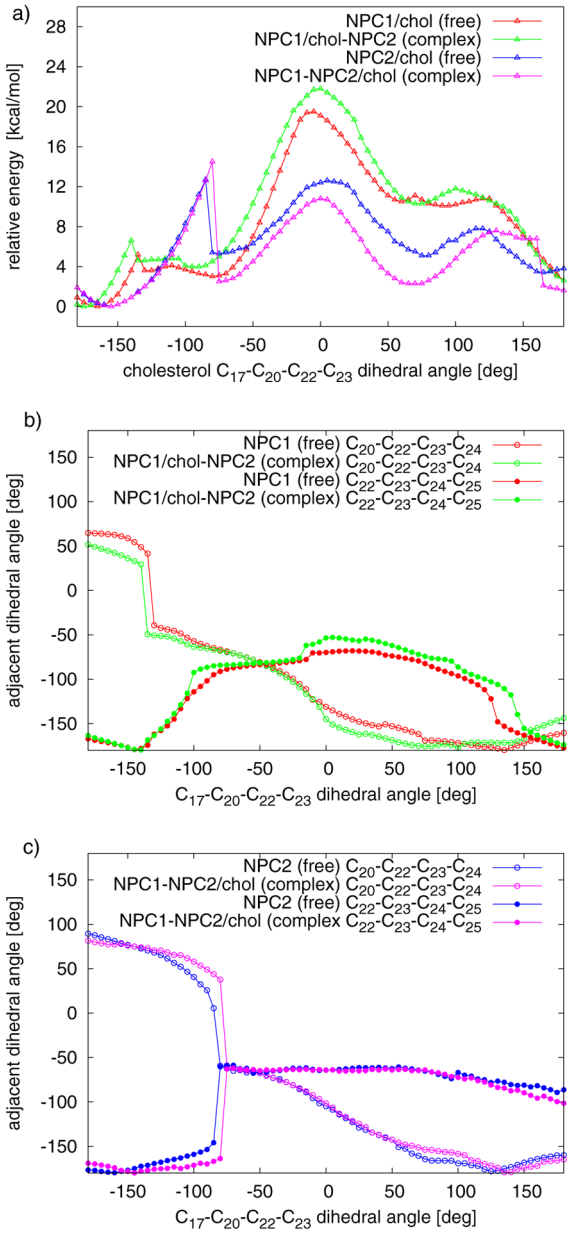

Figure 7. (a) QM/MM isomerization energy barrier plotted as a function of the cholesterol C_{17}−C_{20}−C_{22}−C_{23} dihedral angle inside the NPC1 binding pocket of the free NPC1/chol protein (red line) and the NPC1/chol−NPC2 protein−protein complex (green line) as well as in the NPC2 binding pocket of the free NPC2/chol protein (blue line) and the NPC1−NPC2/chol protein−protein complex (magenta line). The minimum energy for all four species is located between −150° and −175°. The small sharp peaks between −130° and −100° are due to twisting of adjacent C_{20}−C_{22}−C_{23}−C_{24} and C_{22}−C_{23}−C_{24}−C_{25} segments. Values of adjacent dihedral angles are plotted as a function of the primary angle C_{17}−C_{20}−C_{22}−C_{23} (b) for the free NPC1/chol protein (red lines) and the NPC1/chol−NPC2 protein−protein complex (green lines) and (c) for the free NPC2/chol protein (blue lines) and the NPC1−NPC2/chol protein−protein complex (magenta lines).

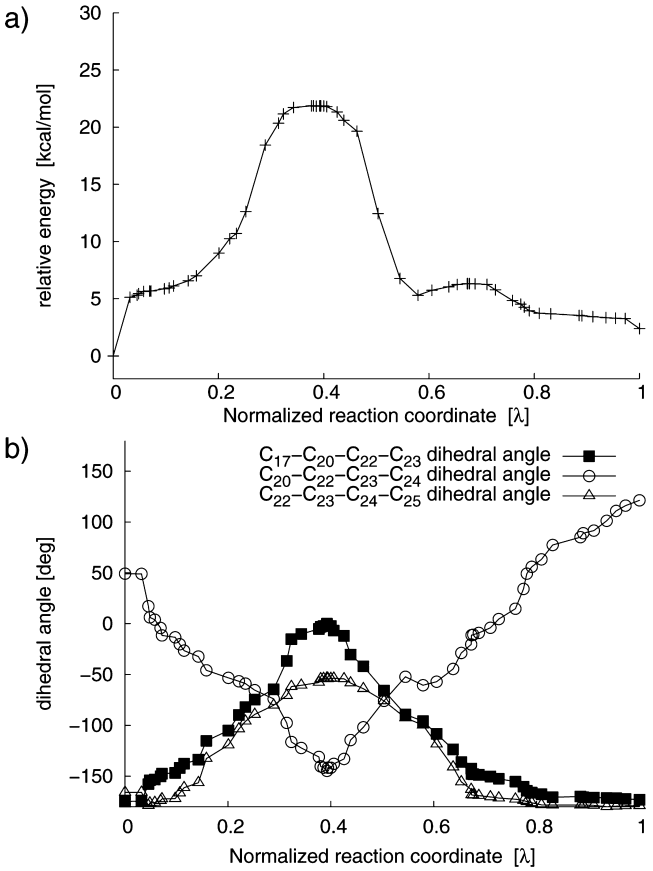

Figure 8. (a) The minimum energy path for the isomerization reaction of NPC1/chol−NPC2 is plotted as a function of the reaction path coordinate (intrinsic) λ. (b) The cholesterol ligand tail twists over the course of the reaction, leading to a simultaneous rearrangement of adjacent dihedral angles C_{17}−C_{20}−C_{22}−C_{23}, C_{20}−C_{22}−C_{23}−C_{24}, and C_{22}−C_{23}−C_{24}−C_{25}.

maximum near ∼0° due to the highly twisted cholesterol tail that is constrained in the protein binding pocket (Supporting Information Figure S2, green line). As the C_{17}−C_{20}−C_{22}−C_{23} segment continues to rotate, the strained sterol tail is relaxed, as evidenced by the decrease in QM energy. The second smaller isomerization barrier near 110° can be attributed to the torsion of the C_{20}−C_{22}−C_{23}−C_{24} and C_{22}−C_{23}−C_{24}−C_{25} segments, which accompanies the twisting of the C_{17}−C_{20}−C_{22}−C_{23} fragment. As the isomerization proceeds, separation between the C_{21} group and nearby amino acids increases as well, leading to a decrease in the total energy. For comparison, the isomerization profile calculated using a purely classical energy function[22] (Supporting Information Figure S2, light blue line) shows a high barrier of approximately 27 kcal/mol, inconsistent with the QM/MM energies and in disagreement with the time scales of 10−100 s predicted by cholesterol transfer assays.[12]

To quantify the energetic effect of internal water on the isomerization barrier in the protein−protein complex, the isomerization was calculated in the absence of water (Supporting Information Figure S2, dashed red line). The highest isomerization barrier near 0° is reduced by approximately 2 to 19.8 kcal/mol. In other words, water molecules in the NPC1 binding pocket stabilize the initial conformation of the ligand and sterically hinder conformational rearrangement. For comparison, the isomerization profile of cholesterol in vacuum has the characteristic three-peak pattern, as observed in the other curves, due to the internal rotation of the neighboring C_{17}−C_{20}−C_{22}−C_{23}, C_{20}−C_{22}−C_{23}−C_{24}, and C_{22}−C_{23}−C_{24}−C_{25} segments. However, the entire curve is significantly lower in energy since the ligand is not constrained by the surrounding protein, and the isomerization in vacuum proceeds via a much

dx.doi.org/10.1021/bi500548f | Biochemistry 2014, 53, 6603−6614

lower barrier of approximately 6 kcal/mol (Supporting Information Figure S2, magenta line).

The isomerization reaction in the NPC1 binding pocket of the protein−protein complex was repeated for three NPC1 mutants, L175Q/L176Q, L175A/L176A, and E191A/Y192A, whose side chains are located in the binding pocket, in the vicinity of the isooctyl tail and near the sterol opening of the NPC1 protein (Supporting Information Figure S1). These mutants have proven to be most deficient in restoring egress of cholesterol from lysosomes.[10,14] The isomerization profiles of these species show that the L175Q/L176Q mutant and the native species both have a total energy barrier near 0° of approximately 20 kcal/mol. For all mutant species, the small peaks near −135° become more pronounced (Figure 9, blue, green, and magenta lines); the wild-type species shows the lowest barrier in this region (Figure 9, red line). A breakdown of the energy profiles for all three mutant species (energy decompositions are shown in Supporting Information Figure S4) reveals structural differences in the binding pockets.

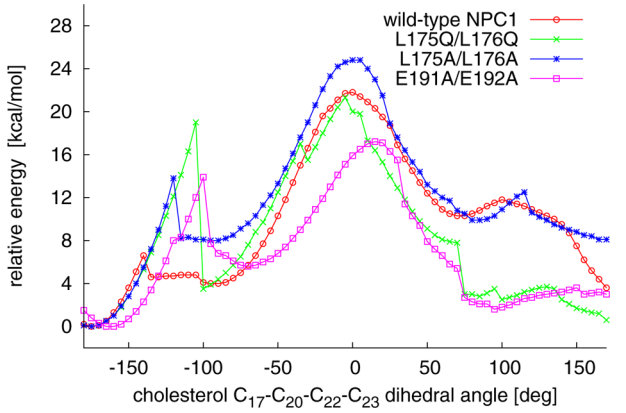

Figure 9. Comparison of the isomerization barriers of cholesterol (C_{17}−C_{20}−C_{22}−C_{23} segment) in the NPC1 binding pocket of the NPC1/chol−NPC2 protein−protein complex for wild-type (red line) as well as for L175Q/176Q (green line), L175A/L176A (dark blue line), and E191A/Y192A (magenta line) mutants. The smaller sharper peaks near −130° are due to twisting of adjacent C_{20}−C_{22}−C_{23}−C_{24} and C_{22}−C_{23}−C_{24}−C_{25} segments caused by the isomerizing C_{17}−C_{20}−C_{22}−C_{23} fragment. The highest overall energy barrier (nearly 25 kcal/mol) is observed for the L175A/L176A mutant (dark blue line) near 0°, whereas the E191A/Y192A mutant (magenta line) shows the lowest overall energy barrier of approximately 17 kcal/mol near 15°. The favorable electrostatic environment in the case of E191A/Y192A mutant, including the fewest number of water molecules near the isooctyl tail (see Supporting Information Figure S1), leads to an overall lower isomerization barrier compared to that of the other three NPC1 species.

In all species, the QM energy comprises the majority of the total energy barrier, and, with the exception of the E191A/Y192A mutant, the QM energy at the barrier is roughly the same (approximately 17 kcal/mol), due to the distorted isomerizing ligand constrained in the binding pocket (Supporting Information Figure S4, green lines). Analysis of the energy decomposition indicates that the L175Q/L176Q mutant shows the largest QM energy near −135°, likely reflecting the energy cost for twisting the adjacent C_{20}−C_{22}−C_{23}−C_{24} and C_{22}−C_{23}−C_{24}−C_{25} fragments in the presence of the polar side chains of Gln amino acids. In L175A/L176A (Figure 9, blue line), the unfavorable nonbonding energies significantly increase the isomerization barrier near 0° to an energy of nearly 25 kcal/mol, likely due to the three water molecules situated between the sterol tail and hydrophobic Ala amino acids (Supporting Information Figure S1). The E191A/Y192A mutant (Figure 9, magenta line) shows the lowest overall energy barrier (16 kcal/mol), slightly shifted to 15°. A comparison of binding pockets (Supporting Information Figure S1) shows that the E191A/Y192A mutant contains one fewer water molecules near the sterol tail. As a result, the isomerizing sterol tail is less sterically hindered and can rotate further (isomerization barrier is slightly shifted as compared to that for other species), and the QM energy at the barrier (approximately 12 kcal/mol) is lower than that of the native NPC1 species and the other two mutants structures. The remainder of the barrier (4 kcal/mol) can be attributed to unfavorable nonbondong energies (Supporting Information Figure S4c).

Isomerization in the NPC2 Binding Pocket. The cholesterol isomerization energy profiles in the NPC2 binding pocket are shown in Figure 7 for the free NPC2 protein (blue line) and for the NPC1−NPC2/chol protein complex (magenta line). In both cases, the highest energy barrier is due to the QM energy arising from the distorted geometry of the ligand tail; the highest energy barrier is the sharp peak located near −100° due to the simultaneous twisting of neighboring dihedral angles C_{20}−C_{22}−C_{23}−C_{24} and C_{22}−C_{23}−C_{24}−C_{25} (Figure 7). The energy barriers (12.6 kcal/mol in the free protein and 14.5 kcal/mol in the protein−protein complex) are both lower than the barriers calculated for the NPC1 protein, indicating a more favorable environment for conformational rearrangement in the NPC2 binding pocket. The energy barrier of 14.5 kcal/mol in the protein−protein complex is compatible with the approximately 10 s binding times measured in bidirectional cholesterol transfer assays.[12]

In the NPC2 binding pocket of the protein−protein complex, the C_{17}−C_{20}−C_{22}−C_{23} dihedral angle after QM/MM energy minimization is −156.5° (Table 2). A small local minimum in both the NPC1 and NPC2 isomerization profiles is observed near 70°, suggesting that a metastable cholesterol geometry may exist in this conformation under certain conditions. Indeed, in classical MD simulations of cholesterol in the NPC2 binding pocket of the protein−protein complex, dihedral angles near 70° were sampled (Figure 4). In addition, Wiest and co-workers report a protein−protein−cholesterol structure in which the cholesterol C_{17}−C_{20}−C_{22}−C_{23} dihedral angle inside the NPC2 binding pocket is near 70°.[8]

The twist of the C_{17}−C_{20}−C_{22}−C_{23} dihedral angle is accompanied by rotations of adjacent C_{20}−C_{22}−C_{23}−C_{24} and C_{22}−C_{23}−C_{24}−C_{25} segments, leading to a clockwise rotation of the C_{21} methyl group toward nearby amino acids Tyr100 and Phe66 (inset in Figure 6). At the highest isomerization barrier, the C_{17}−C_{20}−C_{22}−C_{23} segment is maximally strained. However, unlike in the NPC1 binding pocket, fewer amino acids with polar side-chains, and fewer water molecules near the sterol tail make the electrostatic environment near the sterol tail less energetically repulsive. The cholesterol tail can rearrange more freely and results in an isomerization barrier that is ∼7 kcal/mol lower in energy than the highest barrier calculated in the NPC1 binding pocket.

To check the influence of surrounding water, the isomerization path was recalculated in the absence of water (Supporting Information Figure S3, green dashed line). The energy barriers, as in the case of NPC1 (Supporting Information Figure S3, red lines), are lowered by 2 kcal/mol, demonstrating that internal water molecules have a small but

dx.doi.org/10.1021/bi500548f | Biochemistry 2014, 53, 6603−6614

unfavorable effect on the isomerization energetics in the NPC2 binding pocket.

The relatively lower isomerization barrier calculated for the NPC2 binding pocket, as compared to the NPC1 binding pocket, suggests that the NPC2 binding pocket allows the ligand to have more conformational freedom. The higher degree of conformational freedom in the NPC2 binding pocket could suggest that structural rearrangement prior to ligand transfer is favored for an efficient ligand transfer process. Although the binding strength of the cholesterol ligand in the two protein pockets was not examined in this study, the calculated isomerization barriers of the two proteins may offer some insight into the kinetics of ligand transfer. The lower isomerization barrier calculated for NPC2 could suggest that the NPC2 binding pocket favors a faster structural rearrangement of the ligand, thereby also allowing for a faster entry/exit of sterol ligand into the soluble NPC2 protein, as compared with the time scale of entry/exit into the binding pocket of the membrane-bound NPC1 protein. Indeed, in protein-to-protein cholesterol transfer assays, the transfer of cholesterol from NPC2 occurs rapidly (under 10 min) and reversibly at both 4 and 37 °C. On the other hand, NPC1 behaves differently, slowly (30 min) binding cholesterol at 4 °C and more rapidly (accelerated 140-fold) at 37 °C; at 4 °C, the cholesterol ligand does not dissociate from NPC1 over 2 h.[12] The different binding behavior of the two proteins can be explained by examining the respective binding pockets. The NPC1 binding pocket, with more water molecules near the ligand tail and more polar amino acids, has more unfavorable nonbonding interactions during the isomerization reaction, indicating that the pocket energetically favors ligand binding. On the other hand, the NPC2 binding pocket has fewer water molecules and more hydrophobic amino acids, resulting in a binding pocket in NPC2 with more ligand conformational freedom and weaker ligand binding interactions. Indeed, a conformational change is required for either NPC1 or NPC2 to bind cholesterol.[9,10] Whether this change occurs in the proteins, in the cholesterol ligand, or in both in a concerted rearrangement is still unclear. Since efficient binding of cholesterol is necessary for the transfer of cholesterol from NPC2 to NPC1's N-terminal domain, the energy cost of conformational rearrangements cannot be prohibitively high. If the rearrangement of the cholesterol takes place in the energetically favorable NPC2 binding pocket, either before or after protein docking, then the subsequent transfer of cholesterol to the NPC1 binding pocket can proceed rapidly, freeing NPC2 and allowing the soluble protein to re-enter the cycle of ligand uptake and binding. The subsequent transfer and insertion of cholesterol from the NPC1 binding pocket into the lyosomal membrane presumably follows, although the mechanism for that transfer has not yet been investigated.

CONCLUSIONS

We have investigated the energy barriers associated with conformational changes of cholesterol in the NPC1 and NPC2 binding pockets of the free proteins and the protein−protein complex. In the case of the protein−protein complex, our calculations are based on the proposed hydrophobic hand-off model, in which cholesterol is transferred from the soluble NPC2 protein to the membrane-bound NPC1 following complexation of the two proteins. The protein−protein complex, constructed by aligning the ligand apertures of the individual crystal structures and minimizing the energy of the complex, serves as a working model for simulating cholesterol transfer. In the model, the sterol apertures are aligned, but the binding pockets are bent with respect to one another. In order for the ligand to slide from one binding pocket to the other, a conformational change must occur in the proteins, in the ligand, or in both. Here, we investigated the possibility that the ligand's flexible isooctyl tail undergoes isomerization, either before or after protein docking, to accommodate the bent transfer pathway. We calculated the QM/MM energy barrier associated with this isomerization in the free native NPC1 and NPC2 proteins as well as for the NPC1−NPC2 protein−protein complex.

In the free NPC1/chol binding pocket, cholesterol isomerization proceeds via an energy barrier of 19.5 kcal/mol, whereas in the protein−protein complex, this barrier is increased to 21.8 kcal/mol. Isomerization in the NPC2 binding pocket of the free NPC2/chol protein showed the overall lowest isomerization barrier of 12.6 kcal/mol; in the protein−protein complex, this barrier increases to 14.5 kcal/mol. Isomerization barriers were also calculated for three mutant NPC1−NPC2 species, L175Q/L176Q, L175A/L176A, and E191A/Y192A, whose barriers are approximately 20, 25, and 17 kcal/mol, respectively. On the basis of our calculations, due to the energetically favorable conditions in the NPC2 binding pocket compared to those in NPC1, a conformational rearrangement of cholesterol either before or after protein docking would be favored in the NPC2 binding pocket.

The isomerization energy barriers obtained in our QM/MM calculations of the protein−protein complexes, ranging between 14.5 kcal/mol for native NPC2 and 21.8 kcal/mol for native NPC1, are in agreement with the experimental kinetic rates corresponding to halftimes ranging between 10 and 100 s at 37 C, although these experimentally measured rates should be considered semiquantitative (A. Radhakrishnan, private communication). Therefore, although cholesterol transfer rates are not precisely known, the isomerization barriers calculated here are in accord with the range of measured transfer rates. Our results indicate that cholesterol isomerization within the NPC1 binding pocket is higher in energy than that within the NPC2 binding pocket. This energy difference can be explained by the fact that the NPC1 binding pocket contains more internal water molecules and amino acids with polar side chains, thereby restricting conformational rearrangement for the hydrophobic cholesterol ligand.

Since NPC disease is characterized by disrupted cholesterol trafficking within the lysosome, a quantification of the energetic cost of cholesterol movement between and/or inside the complexed NPC1 and NPC2 proteins is required in order to understand possible causes of disfunction. We observe in our MD calculations, as in those of Wiest and co-workers,[8] that the cholesterol ligand samples different geometries inside the binding pockets of the protein−protein complex, so a conformational rearrangement is likely to play a role in the transfer process. Here, we have not considered the contribution of conformational sampling that may further lower the isomerization (free) energy barrier. Dynamical sampling is likely to lower both isomerization barriers, and, as such, the energy barriers computed here serve as a reference point for subsequent calculations.

Mutagenesis studies indicate a range of mutants that could be responsible for the disrupted cholesterol trafficking within the lysosome. Mutations in either or both the NPC1 or NPC2 proteins that hinder the complexation process, cholesterol

isomerization, or the transfer step could significantly alter the energetics and severely disrupt the trafficking process within the lysosome. In the present study, we focused on the L175A/L176A, L175Q/L176Q, and E191A/Y192A mutants that have shown severely decreased rates of cholesterol transfer. Our calculations show that the isomerization barriers associated with these mutants, as with the wild-type species, are higher than the barriers associated with the NPC2 binding pocket. Therefore, an isomerization reaction in the more favorable NPC2 binding pocket is not affected by mutations in NPC1. Although a comprehensive mutagenesis study was not the focus of this work, calculating the energy barriers associated with other functionally relevant NPC1 and NPC2 mutants would be worthwhile.

Here, we examined the stationary end states of the cholesterol transfer reaction between NPC2 and NPC1. The possibility exists that a conformational rearrangement of cholesterol occurs at any point or over a series of steps along the reaction path linking the two binding pockets. To investigate this scenario, conformational sampling along the QM/MM reaction path connecting the binding pockets of the two NPC proteins should be carried out. Such calculations would give insight not only into enthalpic but also entropic contributions to the free energy of the cholesterol binding and transfer processes. Preliminary calculations for the construction of reaction paths connecting the binding pockets are currently being carried out for the native protein structures.

■ ASSOCIATED CONTENT

Supporting Information

Figure S1: Close-up views of the binding pockets of the native NPC1(NTD) and three mutants studied, L175A/L176A, L175Q/L176Q, and E191A/Y192A. Figure S2: Energy composition of the total QM/MM isomerization energy for the reaction in the NPC1(NTD) binding pocket; the classical isomerization energy profile and the isomerization profile in vacuum are shown for comparison. Figure S3: Comparison of the isomerization energy barriers for the two proteins, with and without water molecules present in the binding pockets. Figure S4: Comparison of the decomposition of the QM/MM isomerization barriers for the three NPC1(NTD) mutants studied. This material is available free of charge via the Internet at http://pubs.acs.org.

■ AUTHOR INFORMATION

Corresponding Author

*E-mail: nadia.elghobashi-meinhardt@fu-berlin.de. Phone: +0049 (30) 838 52128. Fax: +0049 (30) 838 56921.

Funding

Financial support from the Volkswagen Stiftung (grant no. 86 539) is gratefully acknowledged.

Notes

The authors declare no competing financial interest.

■ ACKNOWLEDGMENTS

Acknowledgement is given to H. Runz for insightful discussions involving Niemann−Pick Type C disease. The author thanks M. E. Elghobashi, P. Imhof, and E. W. Knapp for helpful scientific discussions and for proof-reading the manuscript.

■ REFERENCES

(1) Bi, X., and Liao, G. (2010) Cholesterol in Niemann−Pick type C disease. *Subcell. Biochem. 51*, 31935.

(2) Kwon, H. J., Palnitkar, M., and Deisenhofer, J. (2011) The structure of the NPC1L1 N-terminal domain in a closed conformation. *PLoS One 6*, e18722.

(3) Schulze, H., and Sandhoff, K. (2011) Lysosomal lipid storage diseases. *Cold Spring Harb. Perspect. Biol. 3*, a004804.

(4) Runz, H., Dolle, D., Schlitter, A. M., and Zschocke, J. (2008) NPC-db, a Niemann−Pick type C disease gene variation database. *Hum. Mutat. 29*, 345−350.

(5) Helquist, P., and Wiest, O. (2009) Current status of drug therapy development for Niemann−Pick type C disease. *Drugs Future 34*, 315−331.

(6) Goldstein, J. L., Dana, S. E., Faust, J. R., Beaudet, A. L., and Brown, M. S. (1975) Role of lysosomal acid lipase in the metabolism of plasma low density lipoprotein: observations in cultured fibroblasts from a patient with cholesteryl ester storage disease. *J. Biol. Chem. 250*, 8487−8495.

(7) Xu, S., Benoff, B., Liou, H.-L., Loebel, P., and Stock, A. M. (2007) Structural basis of sterol binding by NPC2, a lysosomal protein deficient in Niemann−Pick type C2 disease. *J. Biol. Chem. 282*, 23525−23531.

(8) Estiu, G., Khatri, N., and Wiest, O. (2013) Compuational studies of the cholesterol transport between NPC2 and the N-terminal domain of NPC1 (NPC1(NTD)). *Biochemistry 52*, 6879−6891.

(9) Friedland, N., Liou, H.-L., Lobel, P., and Stock, A. M. (2003) Structure of a cholesterol-binding protein deficient in Niemann−Pick type C2 disease. *Proc. Natl. Acad. Sci. U.S.A. 100*, 2512−2517.

(10) Kwon, H. J., Abi-Mosleh, L., Wang, M. L., Deisenhofer, J., Goldstein, J. L., Brown, M. S., and Infante, R. E. (2009) Structure of N-terminal domain of NPC1 reveals distinct subdomains for binding and transfer of cholesterol. *Cell 137*, 1213−1224.

(11) Wang, J., Chu, B.-B., Ge, L., Li, B.-L., Yan, Y., and Song, B.-L. (2009) Membrane topology of human NPC1L1, a key protein in enterohepatic cholesterol absorption. *J. Lipid Res. 50*, 16531662.

(12) Infante, R. E., Wang, M. L., Radhakrishnan, A., Kwon, H. J., Brown, M. S., and Goldstein, J. L. (2008) NPC2 facilitates bidirectional transfer of cholesterol between NPC1 and lipid bilayers, a step in cholesterol egress from lysosomes. *Proc. Natl. Acad. Sci. U.S.A. 105*, 15287−15292.

(13) Deffieu, M. S., and Pfeffer, S. R. (2011) Niemann−Pick type C1 function requires luminal domain residues that mediate cholesterol-dependent NPC2 binding. *Proc. Natl. Acad. Sci. U.S.A. 108*, 18932−18936.

(14) Wang, M. L., Motamed, M., Infante, R. E., Abi-Mosleh, L., Kwon, H. K., Brown, M. S., and Goldstein, J. L. (2010) Identification of surface residues on Niemann−Pick C2 essential for hydrophobic handoff of cholesterol to NPC1 in lysosomes. *Cell Metab.*, 166−173.

(15) Xie, X., Brown, M. S., Shelton, J. M., Richardson, J. A., Goldstein, J. L., and Liang, G. (2011) Amino acid substitution in NPC1 that abolishes cholesterol binding reproduces phenotype of complete NPC1 deficiency in mice. *Proc. Natl. Acad. Sci. U.S.A. 108*, 15330−15335.

(16) Field, M. J., Bash, P. A., and Karplus, M. (1990) A combined quantum mechanical and molecular mechanical potential for molecular dynamics simulations. *J. Comput. Chem. 11*, 700−733.

(17) Singh, U. C., and Kollman, P. A. (1986) A combined *ab initio* quantum mechanical and molecular mechanical method for carrying out simulations on complex molecular systems: applications to the $CH_3Cl + Cl^-$ exchange reaction and gas phase protonation of polyethers. *J. Comput. Chem. 7*, 718−730.

(18) Warshel, A. (1991) *Computer Modeling of Chemical Reactions in Enzymes and Solutions*, John Wiley & Sons, New York.

(19) Brooks, B. R., Bruccoleri, R. E., Olafson, B. D., States, D. J., Swaminathan, S., and Karplus, M. (1983) CHARMM: a program for macromolecular energy, minimization, and dynamics calculations. *J. Comput. Chem. 4*, 187−217.

(20) Cournia, Z., Vaiana, A. C., Ullmann, G. M., and Smith, J. C. (2004) Derivation of a molecular mechanics force field for cholesterol. *Pure Appl. Chem. 76*, 189−196.
(21) Cournia, Z., Smith, J. C., and Ullmann, M. (2005) A molecular mechanics force field for biologically important sterols. *J. Comput. Chem. 26*, 1383−1399.
(22) MacKerell, A. D., Jr., Bashford, D., Bellott, M., Dunbrack, R. L., Jr., Evanseck, J. D., Field, M. J., Fischer, S., Gao, J., Guo, H., Ha, S., Joseph-McCarthy, D., Kuchnir, L., Kuczera, K., Lau, F. T. K., Mattos, C., Michnick, S., Ngo, T., Nguyen, D. T., Prodhom, B., Reiher, W. E., III, Roux, B., Schlenkrich, M., Smith, J. C., Stote, R., Straub, J., Watanabe, M., Wiórkiewicz-Kuczera, J., Yin, D., and Karplus, M. (1998) All-atom empirical potential for molecular modeling and dynamics studies of proteins. *J. Phys. Chem. B 102*, 3586−3616.
(23) Jorgensen, W., Chandrasekhar, J., Madura, J., Impey, R., and Klein, M. (1983) Comparison of simple potential functions for simulating liquid water. *J. Chem. Phys. 79*, 926−935.
(24) Elstner, M., Porezag, D., Jungnickel, G., Elsner, J., Haugk, M., Frauenheim, T., Suhai, S., and Seifert, G. (1998) Self-consistent-charge density functional tight-binding method for simulations of complex materials properties. *Phys. Rev. B 58*, 7260−7268.
(25) Cui, Q., Elstner, M., Kaxiras, E., Frauenheim, T., and Karplus, M. (2001) A QM/MM implementation of the self-consistent charge density functional tight binding (SCC-DFTB) method. *J. Phys. Chem. B 105*, 569−585.
(26) Pu, J., Gao, J., and Truhlar, D. G. (2004) Combining self-consistent-charge density-functional tight-binding (SCC-DFTB) with molecular mechanics by the generalized hybrid orbital (GHO) method. *J. Phys. Chem. A 108*, 5454−5463.
(27) Elstner, M., Frauenheim, T., Kaxiras, E., Seifert, G., and Suhai, S. (2000) A self-consistent-charge density functional based tight-binding scheme for large biomolecules. *Phys. Status Solidi B 217*, 357−376.
(28) Zhou, H., Tajkhorshid, E., Frauenheim, T., Suhai, S., and Elstner, M. (2002) Performance of the AM1, PM3, and SCC-DFTB methods in the study of conjugated Schiff base molecules. *Chem. Phys. 277*, 91−103.
(29) Phillips, J. C., Braun, R., Wang, W., Gumbart, J., Tajkhorshid, E., Villa, E., Chipot, C., Skeel, R. D., Kale, L., and Schulten, K. (2005) Scalable molecular dynamics with NAMD. *J. Comput. Chem. 26*, 1781−1802.
(30) Ryckaert, J. P., Ciccotti, G., and Berendsen, H. J. C. (1977) Numerical integration of the cartesian equations of motion of a system with constraints: molecular dynamics of n-alkanes. *J. Comput. Phys. 23*, 327−341.
(31) Pastor, R. W., Brooks, B. R., and Szabo, A. (1988) An analysis of the accuracy of Langevin and molecular dynamics algorithms. *Mol. Phys. 65*, 1409−1419.
(32) Fischer, S., and Karplus, M. (1992) Conjugate peak refinement: an algorithm for finding reaction paths and accurate transition states in systems with many degrees of freedom. *Chem. Phys. Lett. 194*, 252−261.
(33) Case, D. A., Darden, T. A., Cheatham, T. E., Simmerling, C. L., Wang, J., Duke, R. E., Luo, R., Walker, R. C., Zhang, W., Merz, K. M., Roberts, B., Wang, B., Hayik, S., Roitberg, A., Seabra, G., Kolossvary, I., Wong, K. F., Paesani, F., Vanicek, J., Liu, J., Wu, X., Brozell, S. R., Steinbrecher, T., Gohlke, H., Cai, Q., Ye, X., Wang, J., Hsieh, M., Cui, G., Roe, D. R., Mathews, D. H., Seetin, M. G., Sagui, C., Babin, V., Luchko, T., Gusarov, S., Kovalenko, A., and Kollman, P. A. (2010) *AMBER 11*, University of California, San Francisco, CA.

■ NOTE ADDED AFTER ASAP PUBLICATION

This paper published ASAP on October 10, 2014. The Supporting Information file was replaced and the revised version was reposted on October 13, 2014.